nature communications

Article

https://doi.org/10.1038/s41467-025-61336-6

Preference of negatively charged membranes in magnesium and lithium separation by nanofiltration

Received: 12 April 2025

Accepted: 16 June 2025

Published online: 01 July 2025

Check for updates

Lulu Liu[1,2], Shihong Lin[3], Xinyi Xu[1,2], Yinhua Wan[2,4] ✉, Weijie Song[1] & Jianquan Luo[1,2] ✉

Despite the traditional co-ion competition theory suggesting that positively charged nanofiltration (NF) membranes are best for Li^+/Mg^{2+} separation, practical applications predominantly utilize negatively charged membranes. Furthermore, most biological ion channels in nature are characterized by negatively charged functional groups. To address this theoretical discrepancy, we conducted a comprehensive study that integrates experimental data with molecular dynamics simulations to explore the transport behavior of Mg^{2+} and Li^+ through negatively charged NF membranes. When using mixed salt solutions as feed, NF membranes with strong negative charges and small pore sizes achieved a high rejection of Mg^{2+} (>90%), with a Li^+ rejection as low as −53.2%. This remarkable selectivity is primarily driven by the proposed ion competition mechanism termed counter-ion competition. For weakly hydrated monovalent counter-ions, such as Li^+, the enrichment of strongly hydrated counter-ions like Mg^{2+} near the membrane pores facilitates the dehydration of Li^+ at the pore entrance, thereby reducing its size exclusion effect. Simultaneously, this dehydration enhances the electrostatic interaction between Li^+ and the negatively charged NF membrane, resulting in high permeability of Li^+. Our work advances the understanding of ion-selective transport in NF membranes, offering mechanistic guidance for developing high-performance NF membranes for Li^+/Mg^{2+} separation.

Nanofiltration (NF), which utilizes size sieving and the Donnan effect as the primary separation mechanisms, is recognized as a promising membrane technology for ion-selective separation[1–3]. Despite its potential, further improvements in separation selectivity are still needed. Taking lithium extraction from salt lakes as an example[4], interfering ions like Mg^{2+} (hydrated radius of 4.5 Å) exhibit a hydrated radius nearly identical to that of Li^+ (hydrated radius of 3.8 Å)[5]. This similarity in hydrated radii poses significant challenges for efficient ion-selective separation by NF at the sub-nanometer scale[6,7]. Moreover, many brines have an Mg^{2+}/Li^+ mass ratio (MLR) greater than 20, and contain high levels of total dissolved solids (e.g., Na^+ and Ca^{2+}), which can interfere with the separation process and contribute to membrane fouling[8]. Such complexities are regarded as the primary obstacles hindering the efficacy of direct lithium extraction from brines by NF.

Strategies such as enhancing the positive charge of NF membranes, incorporating Li^+ channels, and optimizing membrane pore size distribution have been proposed to improve the Li^+/Mg^{2+} separation efficiency[9–13]. For instance, highly positively charged polyethyleneimine

[1]State Key Laboratory of Biopharmaceutical Preparation and Delivery, Institute of Process Engineering, Chinese Academy of Sciences, Beijing, PR China. [2]School of Chemical Engineering, University of Chinese Academy of Sciences, Beijing, PR China. [3]Department of Civil and Environmental Engineering and Department of Chemical and Biomolecular Engineering, Vanderbilt University, Nashville, TN, USA. [4]Ganjiang Innovation Academy, Chinese Academy of Sciences, Ganzhou, PR China. ✉e-mail: yhwan@ipe.ac.cn; jqluo@ipe.ac.cn

(PEI)-based membranes are claimed to exhibit strong electrostatic repulsion against Mg^{2+} compared to Li^+, thereby enhancing Li^+/Mg^{2+} separation performance via intensified Donnan exclusion[14]. The $MgCl_2$ rejection of the PEI-based membrane can be as high as 97.4%. Additionally, a triplet quaternary ammonium monomer, engineered to carry a stronger positive charge, was polymerized with trimesoyl chloride (TMC), resulting in an NF membrane with enhanced positive charge density[15]. Recent studies have increasingly focused on strengthening the Donnan exclusion and modulating membrane structure through post-modification techniques (such as grafting ionic liquids or strong electrolytes) to further improve Li^+/Mg^{2+} selectivity ($S_{Li^+/Mg^{2+}}$)[16–19].

We summarize literature data on the performance of NF membranes capable of efficiently separating Li^+/Mg^{2+} mixtures, which are compiled in Fig. 1a. Positively charged membranes (i.e., isoelectric point (IEP) greater than 6) can achieve very high Mg^{2+} rejections but their Li^+ rejections are moderate (from −10% to 80%). In comparison, negatively charged membranes (IEP < 6) can also achieve high Mg^{2+} rejection but with much lower Li^+ rejection, while maintaining an $S_{Li^+/Mg^{2+}}$ comparable to that of positively charged membranes. For two NF processes with the same MLR and high $S_{Li^+/Mg^{2+}}$ but different ion rejections, high lithium purity can still be achieved. However, Li^+ rejection determines lithium recovery, with low Li^+ rejection leading to higher lithium recovery (Fig. 1b). Herein, lithium recovery is defined as the mass fraction of Li^+ in the feed that is eventually recovered in the permeate, while lithium purity is defined as the mass fraction of Li^+ cations in the permeate. Negatively charged dense NF membranes (with a molecular weight cutoff, MWCO < 300 Da) show better potential for Li^+/Mg^{2+} separation than positively charged membranes in terms of Li^+ rejection (Fig. 1a, b and Supplementary Figs. 1 and 2).

However, the research on positively charged NF membranes for Li^+/Mg^{2+} separation has attracted increasing attention, driven by the conventional belief that co-ion competition benefits selectivity[20]. Specifically, when the positively charged membrane is used to separate Li^+/Mg^{2+} mixtures, Li^+, which is a co-ion (i.e., an ion with the same charge sign as the membrane), is more permeable than the competing co-ion Mg^{2+} due to the lower charge density and higher diffusional mobility of Li^+ (Fig. 1c)[21,22]. The combined effect of co-ion competition and Donnan equilibrium results in a lower Li^+ rejection in mixtures with Mg^{2+} compared to single LiCl solutions. Meanwhile, the significant difference in Li^+ and Mg^{2+} rejection observed in their mixtures when using negatively charged NF membranes poses a challenge for existing theories. The conventional NF theory suggests that, in negatively charged dense membranes, the interception of Mg^{2+} induces a potential gradient that facilitates the transport of co-ions (Cl^- in this case), which is then followed by the transport of counter-ions (Li^+) with lower steric hindrance to maintain charge neutrality in the permeate[23]. Although co-ion partitioning theory supports the preferential partitioning of Cl^- in negatively charged membranes (Fig. 1d)[24], the preferential permeation of Cl^- should, in principle, be more pronounced in positively charged NF membranes due to the electrostatic attraction between Cl^- and the membrane. However, this does not lead to a significant decrease in Li^+ rejection for positively charged NF membranes (Fig. 1a). According to traditional filtration theory, co-ion competition occurs in charged membranes (Fig. 1c). However, for negatively charged NF membranes used in Li^+/Mg^{2+} separation, Cl^- is the only co-ion present, with no competing co-ions. This raises a fundamental question: is there counter-ion competition between Mg^{2+} and Li^+ in negatively charged membranes? A comprehensive theoretical framework is urgently needed to elucidate this phenomenon.

Furthermore, a membrane with a charge similar to the ions being separated is not a prerequisite for achieving high selectivity. For instance, biological ion channels, despite their negative charges, can achieve exceptionally high selectivity for Na^+ or K^+ through the synergistic effects of sub-nanometer pore size, optimal charge density, and specific binding sites[25–28]. Therefore, to investigate why negatively charged membranes are more effective for separating Li^+ and Mg^{2+} in NF, we compare commercially available negatively charged NF membranes with self-prepared PEI-based NF membranes, both of which have been widely studied for lithium extraction from brines. Using a simple Li^+/Mg^{2+} mixture as the feed, we systematically examine the impact of membrane charge properties on the separation behavior of Mg^{2+} and Li^+. We conduct both experiments and simulations to evaluate the effects of co-existing cations and membrane structures on the Li^+/Mg^{2+} separation performance of negatively charged NF membranes. We then investigate the impacts of MLR and solution pH on Li^+ rejection in mixed salt systems. Finally, we extend the application of the negatively charged NF membrane to lithium extraction from brines, highlighting its advantages in separation efficiency. This study not only resolves the theoretical puzzle of ion competition mechanisms in selective transmembrane transport but also provides fundamental insights for developing advanced ion separation membrane materials with high selectivity.

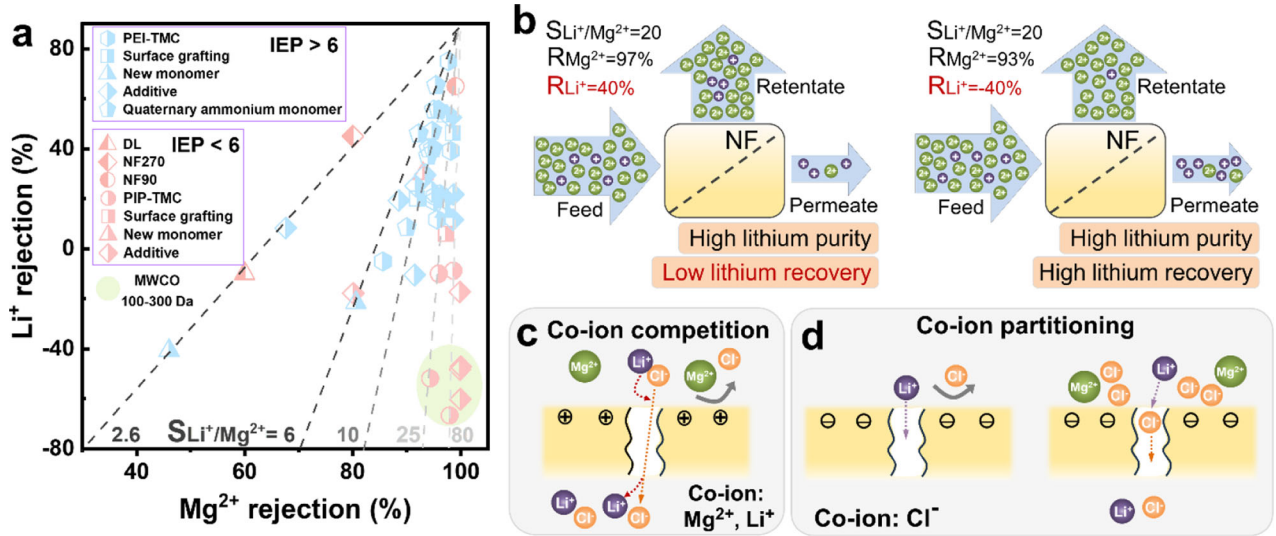

Fig. 1 | Lithium separation performance and transport mechanisms in selective membranes. a Li^+ and Mg^{2+} rejections of the membrane reported in the literature (data source available in Supplementary Table 1). Each dashed line connects data points from the same $S_{Li^+/Mg^{2+}}$. **b** Effect of $S_{Li^+/Mg^{2+}}$ and ion rejections on lithium purity and lithium recovery. Schematic illustration of the **c** co-ion competition and **d** co-ion partitioning.

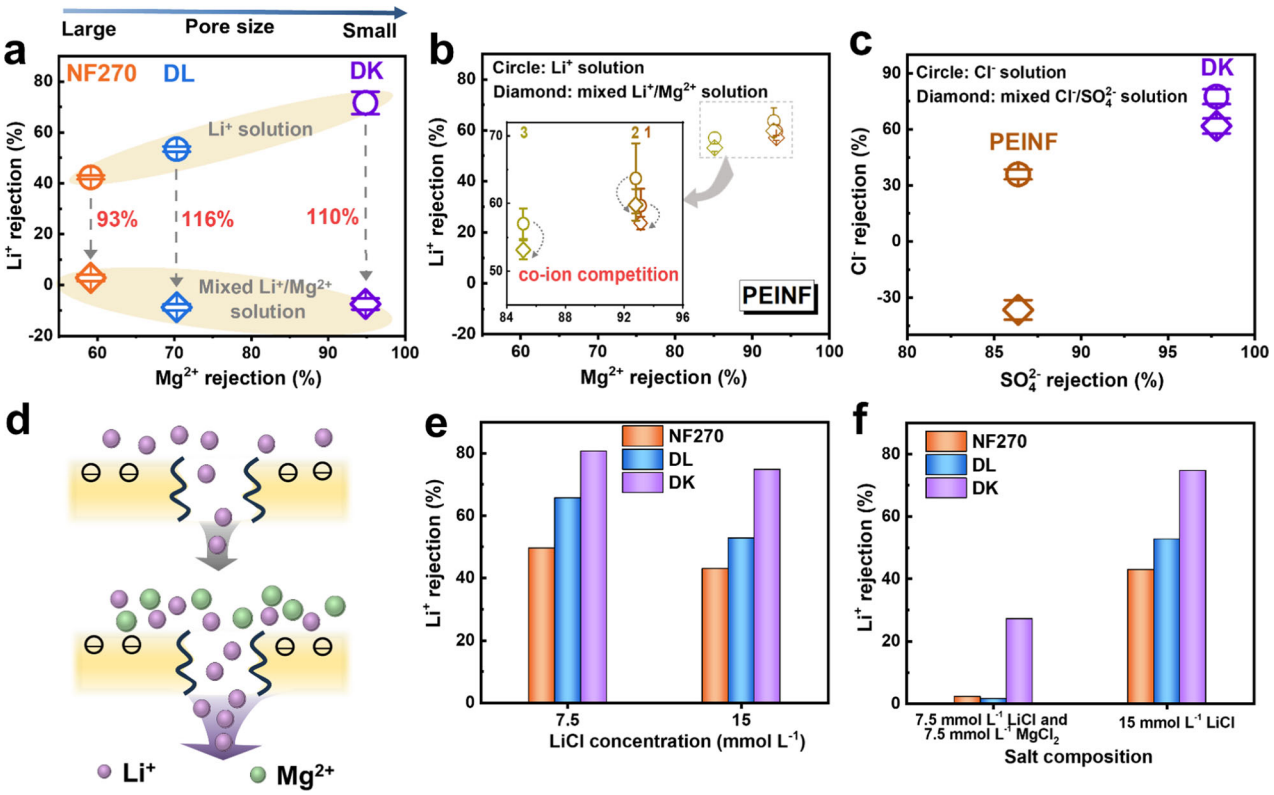

Fig. 2 | Ion sieving performance of differently charged membranes. Ion rejections of (**a**) negatively charged membranes and (**b**) positively charged membranes during filtration of different ions (the mixed Li^+/Mg^{2+} solution includes 15 mmol L^{-1} $MgCl_2$ and 15 mmol L^{-1} LiCl). The inset represents an enlarged view showing finer details of the main figure. Dotted arrows serve as visual guidance. **c** Anion rejection of the DK and PEINF membranes under different solution conditions. The data are presented as mean ± standard deviations (SD), $n = 3$. Error bars in all figures represent SD calculated using the STDEV formula. **d** Schematic diagram of the rejection of different ion solutions by negatively charged NF membranes. Effect of **e** salt concentration and **f** ion composition on Li^+ rejection of negatively charged membranes.

Results

Ion separation performance of differently charged membranes

The cation separation performance of negatively charged membranes was tested against positively charged membranes using either the single Li^+ solution or Li^+/Mg^{2+} mixtures (with Cl^- as the anion) by the cross-flow filtration. The NF membranes with different charge properties were either commercially available or custom-made through interfacial polymerization (Supplementary Table 2), with the custom-made membranes labeled PEINF1, PEINF2, and PEINF3. The influence of membrane permeability and separation layer thickness on ion separation performance was excluded to the greatest extent possible (Supplementary Figs. 3 and 4). The zeta potential measurements suggest that the IEP of commercial DK, DL, and NF270 membranes was all below 4 (Supplementary Fig. 5). Consequently, the rejections followed the typical order for negatively charged NF membranes: $Na_2SO_4 > MgCl_2 > NaCl > LiCl$ (Supplementary Fig. 6a)[29,30]. Among the PEI-based NF membrane, PEINF1, which exhibited an amine density 16 times higher than that of the DK membrane (Supplementary Fig. 6b), demonstrated strong positive charge characteristics (with an amine group density of 905 μmol m^{-2}). Given its exceptional surface chemical properties, the PEINF1 membrane was employed as the representative sample of the PEINF series for all subsequent characterization and performance evaluation in this study.

During mixed salt filtration, negatively charged membranes (such as DK) showed excellent Li^+/Mg^{2+} selectivity (Supplementary Fig. 7). Compared to the filtration of LiCl alone, the presence of Mg^{2+} in mixed salt filtration significantly reduced the Li^+ rejection (Fig. 2a), with the most pronounced decrease observed when using the DK membrane (where the Li^+ rejection decreased by 110%). Due to its small pore size, the DK membrane achieved a high rejection of Mg^{2+} (>90%) while achieving a negative rejection of Li^+, indicating a marked ion competition effect (defined as ions with the same charge sign but different valence and size competing to pass through the membrane in a mixed salt solution). This ion competition effect was observed in all negatively charged membranes for the separation of divalent cations (Ca^{2+} or Mg^{2+}) and monovalent cations (Na^+ and Li^+) in chloride salt systems, where the presence of divalent cations significantly reduced the rejection of monovalent cations (Supplementary Fig. 8). Conversely, the positively charged PEI-based NF membranes maintained high Li^+ rejection even under co-ion competition (Fig. 2b). This trend is also evident in other commercial negatively charged NF membranes and reported positively charged NF membranes (Supplementary Fig. 9). Specifically, the presence of Mg^{2+} more readily reduces Li^+ rejection in negatively charged NF membranes, except in cases where pore sizes are particularly small (see detailed discussion below). While compared with single salt NaCl filtration, the PEI-based NF membranes exhibited obvious ion competition in mixed $NaCl/Na_2SO_4$ filtration, where the introduction of SO_4^{2-} resulted in negative rejection of Cl^- (Fig. 2c and Supplementary Fig. 10). This indicates that lower-charged counter-ions (ions with opposite charges to the membrane) permeate more rapidly through the charged membrane in the mixture than in a single solution (Fig. 2d).

Previous studies have reported that counter-ions can adsorb onto the membrane surface, thereby reducing the effective membrane charge (Supplementary Figs. 11 and 12)[31–33]. In our experiments, negatively charged NF membranes exhibit high Li^+ rejection (50-80%) in a single LiCl solution, with only a slight decrease as salt concentration increases (Fig. 2e). This suggests that the Donnan effect is not the dominant mechanism in Li^+/Mg^{2+} separation, as electrostatic screening would otherwise significantly reduce Li^+ rejection. Instead, the

https://doi.org/10.1038/s41467-025-61336-6

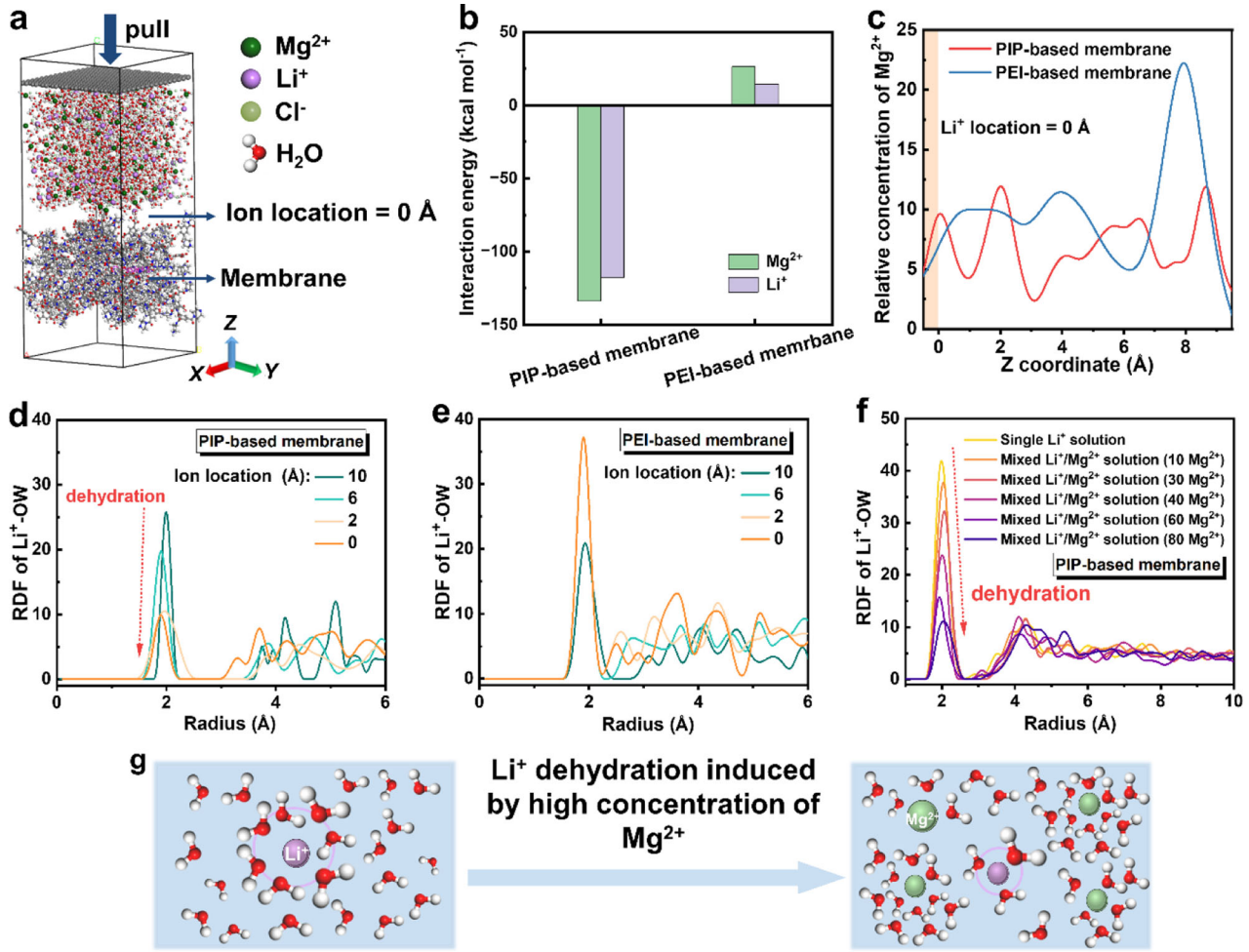

Fig. 3 | Theoretical calculation and analysis of ion transport mechanism. **a** Lateral view of the simulation box. The red, blue and white spheres represent O, N and H atoms, respectively. **b** Interaction energy between counter-ion and membrane. **c** Relative concentration of Mg^{2+} on the surface of PIP-based membrane and PEI-based membrane along the Z coordinate (the yellow area corresponds to the membrane location). RDF of oxygen in water molecules (OW) around Li^+ within **d** PIP-based membrane and **e** PEI-based membrane. **f** Effect of Mg^{2+} concentration on RDF for Li^+-OW. For the molecular dynamics simulation, different number Mg^{2+} were added into the simulation box to represent varying bulk concentrations. The red arrows show the downward trend. **g** Response mechanisms of ionic composition to ionic hydration structure.

observed variations in Li^+ rejection in response to changes in ion composition indicate the influence of an ion competition effect (Fig. 2f). The sharp decline in Li^+ rejection observed in negatively charged membranes induced by the presence of Mg^{2+} cannot be explained by the previously proposed theory of preferential Cl^- partitioning. This is because, theoretically, the electrostatic attraction between positively charged membranes and Cl^- would promote Cl^- partitioning, resulting in a more significant reduction in Li^+ rejection. However, compared to single-salt solutions, the Li^+ rejection in mixed-salt solutions by positively charged membranes decreases much less than that by negatively charged membranes (Figs. 2a, b). Given that negatively charged NF membranes are employed for cation separation, we attribute this phenomenon to counter-ion competition (see the next section for further discussion). In conclusion, the counter-ion competition effect in negatively charged dense NF membranes significantly enhances Li^+/Mg^{2+} separation in mixed salt solutions—an effect that cannot be fully explained by conventional theories, such as Donnan exclusion and Cl^- preferential partitioning in Li^+ permeation.

Mechanism of counter-ion competition

Apart from the widely accepted Donnan effect, ion dehydration is often invoked to explain anomalous ion transport across membranes[23,34]. Here, we conducted molecular dynamic simulations to elucidate the interactions between Mg^{2+} and Li^+ with the membrane, as well as key hydration structure parameters under various solution conditions, to reveal the interaction energies between the ions and the membrane (Fig. 3a). As the membrane charge transitions from negative (PIP-based membrane) to positive (PEI-based membrane) (Supplementary Fig. 13), the electrostatic interactions between the membrane and the cations vary from attractive to repulsive, thereby impeding the cations from approaching the membrane surface (Fig. 3b). This shift is notably accompanied by a differential concentration distribution of Mg^{2+} along the Z-axis (the direction normal to the membrane) near the membrane surface. Under the influence of strong electrostatic attraction, Mg^{2+} ions tend to accumulate on the surface of the PIP-based membrane (Fig. 3c). The pore size distributions of the PIP-based and PEI-based membranes in the simulation were deliberately matched (Supplementary Fig. 14) to exclude the influence of size exclusion on ionic diffusion.

We established the radial distribution functions (RDF, g(r)) between Li^+ and the oxygen atoms of water (OW) in the mixed solution, with the peak intensities reflecting the number of water molecules within the ion hydration shells. The RDF was calculated for ions and OW at various locations. The RDF of Li^+-OW has a significantly lower peak intensity as Li^+ moves towards the surface of the negatively charged membrane (Fig. 3d), whereas an opposite trend was observed

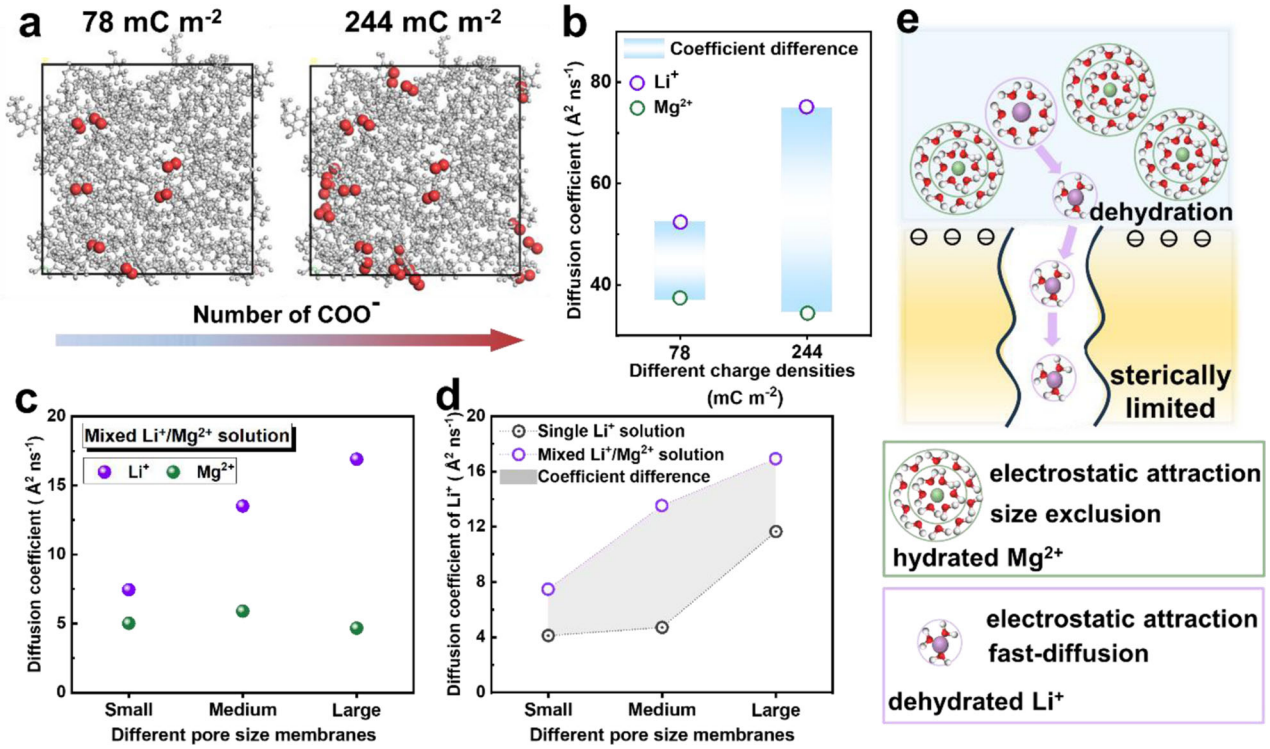

Fig. 4 | Investigation of the factors affecting counter-ion competition by molecular dynamics simulation. a 78 mC m^{-2} and 244 mC m^{-2} charged membranes with carboxylate end groups (red). Effect of **b** membrane charge and **c** pore size on diffusion coefficients of Li^+ and Mg^{2+} in confined space near the membrane surface. Bulk solution was the $LiCl/MgCl_2$ mixture. **d** Diffusion coefficient of Li^+ in confined space near the membrane surface of NF membranes with different pore sizes. **e** Schematic illustration of the possible mechanism for Mg^{2+} density enhancing the Li^+/Mg^{2+} separation in diffusion process.

for positively charged membranes (Fig. 3e). This observation suggests that the structure of water molecules within the Li^+ hydration shell is affected only when Mg^{2+} ions accumulate as counter-ions at the membrane surface. In other words, the accumulation of the divalent counter-ions (Mg^{2+}) near the membrane surface leads to partial dehydration of the weakly hydrated Li^+ (Supplementary Fig. 15). Correspondingly, we observed a further attenuation of the first hydration peak of Li^+ with increasing Mg^{2+} concentrations in the separation with the negatively charged membrane (Fig. 3f). This phenomenon is primarily driven by the increased accumulation of Mg^{2+} near the membrane pores, which intensifies the competition for bound water molecules with Li^+ (as illustrated in Fig. 3g). This dehydration effect not only reduces the size exclusion of Li^+ but also potentially amplifies its electrostatic attraction to the membrane (Supplementary Fig. 16, with an increase of 21 kcal mol^{-1} in electrostatic attraction energy), resulting in enhanced Li^+ permeation. The electrostatic attraction between the Li^+ and membrane pore wall may overcome the dehydration energy barrier[25], leading to further dehydration of Li^+ and thus facilitating its transport through the channel. However, when the mean effective pore size of the negatively charged membrane is sufficiently small (e.g., the effective pore size of NF90 is 4.3 Å), the transport of dehydrated Li^+ will be limited, resulting in a high Li^+ rejection by the membrane (Supplementary Fig. 17). During the separation process, Mg^{2+}, which is enriched in the confined space near the membrane surface, competes for water in the hydration shell of Li^+, facilitating the penetration of Li^+ through the negatively charged membrane. We refer to this phenomenon as counter-ion competition, which can also be regarded as counter-ion promotion in the context of ion-selective separation applications.

The counter-ion competition effect can be further intensified through the synergistic interplay of charge density and pore size[35,36]. Membranes with varying charge intensities were simulated by selectively deprotonating carboxyl groups, as illustrated in Fig. 4a. Although the deprotonation sites were chosen arbitrarily, they were deliberately concentrated on the membrane surface. The diffusion coefficients of ions in the $LiCl/MgCl_2$ mixture in the confined space near the surface of the negatively charged membrane are reported in Fig. 4b. As the membrane becomes more negatively charged (from −78 to −244 mC m^{-2}), the diffusion coefficient of Li^+ in confined space near the membrane surface increases significantly (determined from the mean squared displacement (MSD) curves shown in Supplementary Fig. 18), indicating that Li^+ enters the membrane pores more rapidly. Additionally, with the increase in membrane charge density, the strong attraction of cations with the negatively charged membrane leads to the accumulation of Mg^{2+} on the membrane surface, and accordingly, this strong adsorption restricts its diffusion on the membrane surface, resulting in a slight decrease in Mg^{2+} diffusion coefficient in confined space near the membrane surface. Notably, the differential interactions between the membrane and the cations amplify the disparity in diffusion coefficients between Li^+ and Mg^{2+}, with a larger difference corresponding to higher membrane selectivity.

Furthermore, the diffusion ability of counter-ions on the membrane surface is also influenced by the pore size of the PIP-based membrane (model shown in Supplementary Fig. 19). The smaller pores of the membrane exhibited a stronger resistance to Li^+ diffusion, maintaining a low diffusion coefficient for Li^+ even under counter-ion competition. Conversely, for membranes with larger pores, the weaker size exclusion allowed for a consistently high Li^+ diffusion coefficient (Fig. 4c and Supplementary Fig. 20). Due to the strong size exclusion of Mg^{2+}, there is no obvious difference in the diffusion coefficients across membranes with varying pore sizes. Only membranes with appropriately sized pores can leverage the counter-ion competition effect to amplify the difference in Li^+ diffusion coefficients between single and mixed salt solutions (Fig. 4d and Supplementary Fig. 21), aligning with experimental observations (Supplementary Fig. 22). This highlights the critical role of the interplay between membrane charge and pore size

https://doi.org/10.1038/s41467-025-61336-6

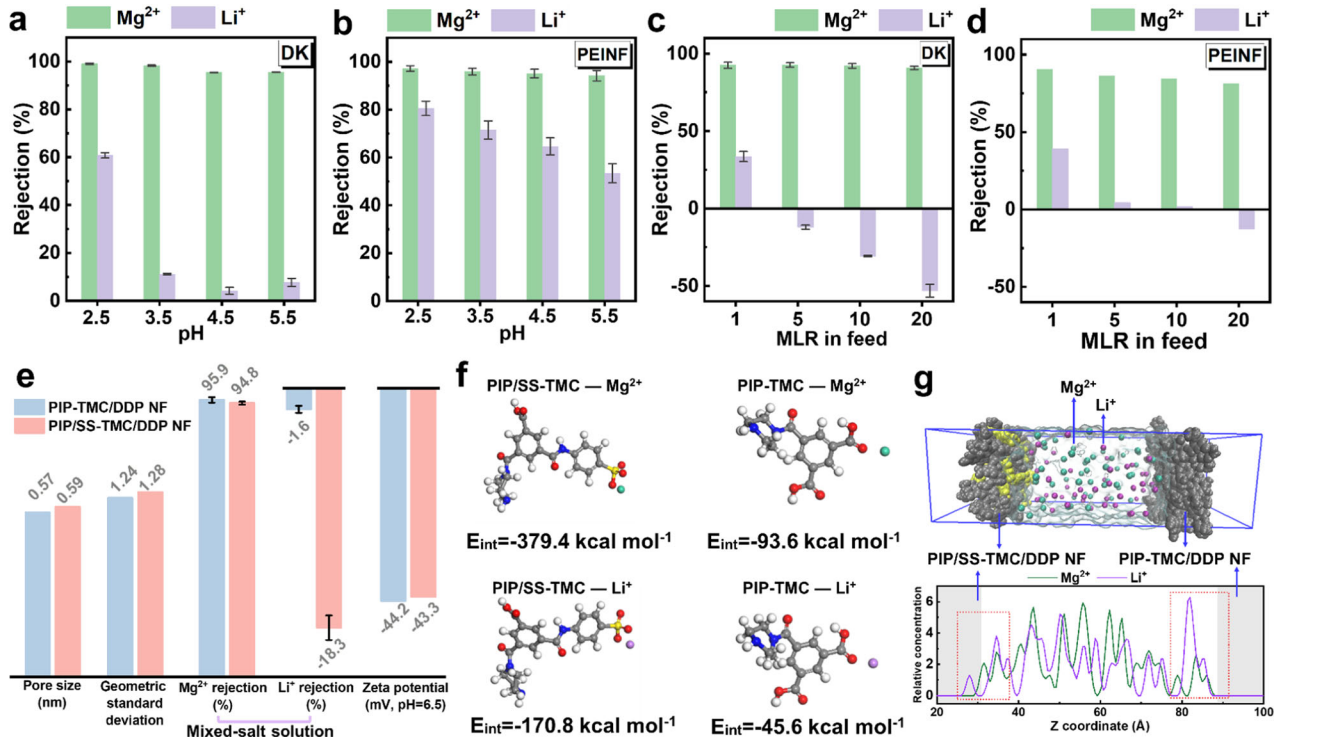

Fig. 5 | Effect of solution conditions and membrane properties on the separation performance for differentiating Li^+ and Mg^{2+}. Effect of pH on the ionic rejection of (**a**) DK and (**b**) PEINF when filtrating 15 mmol L^{-1} $MgCl_2$ and 15 mmol L^{-1} LiCl mixture. Variation of the ion rejections of (**c**) DK and (**d**) PEINF with respect to the MLR in the feed (Concentration: 2000 ppm). **e** Pore size, geometric standard deviation, ion rejection (Feed: 15 mmol L^{-1} $MgCl_2$ and 15 mmol L^{-1} LiCl mixture) and zeta potential of the resulting membranes. **f** The optimized structure and corresponding calculated interaction energy between the membrane unit and ions. **g** Molecular snapshots and concentration profiles (the gray regions correspond to membrane locations). The data are presented as mean ± SD, $n = 3$.

in enhancing the counter-ion competition effect on the membrane surface. Due to the size (steric) exclusion, the strong electrostatic attraction between the membrane and the highly hydrated counter-ion (Mg^{2+}) leads to the accumulation of Mg^{2+} ions on the membrane surface (pore entrance), causing the partial dehydration of the weakly hydrated counter-ion (Li^+). This reduction in hydrated diameter of Li^+, combined with increased electrostatic attraction, facilitates rapid permeation of Li^+, thereby enhancing the $S_{Li^+/Mg^{2+}}$ (Fig. 4e).

Effects of solution chemistry on counter-ion competition

The above analysis suggests that competitive ion dehydration emerges as the primary driving force behind the counter-ion competition effect, while the Donnan effect amplifies the facilitated permeation resulting from ion dehydration, as observed with Li^+. Given the significant influence of pH, ion composition, and membrane charge on the Donnan exclusion[37,38], we examined the impact of these three key factors on the counter-ion competition effect. The ionic rejection of the DK (negatively charged) and PEINF membrane (positively charged) was tested using a LiCl/$MgCl_2$ mixture. The pH-dependent rejection of co-existing cations reveals a marked decrease in Li^+ rejection (from 60.7% to only 7.7%) with the DK membrane when pH increased (from 2.5 to 5.5), while Li^+ rejection as a co-ion on the PEINF membrane shows much substantially less decline (Fig. 5a, b). The deprotonation of amine groups on the polyamide active layer at higher pH enhances the electrostatic attraction between cations and the negatively charged membrane, thereby increasing the interfacial enrichment of Mg^{2+} and thus the dehydration of Li^+. Both reduced size exclusion and enhanced electrostatic attraction due to Mg^{2+}-enhanced dehydration facilitate Li^+ ion permeation. For the positively charged membrane, the deprotonation of amine groups also reduces the electrostatic repulsion against Li^+. However, the more pronounced decrease in Li^+ rejection as a counter-ion for the negatively charged membrane emphasizes that the counter-ion competition effect plays a more significant role in membrane selectivity than the co-ion competition effect.

We further investigated the separation performance of the NF membranes under varying MLR conditions. With a constant total salt concentration of 2000 ppm, increasing the MLR from 1:1 to 20:1 resulted in a reduction in Li^+ rejection by the PEINF membrane from 39.3% to −12.7%, while the DK membrane exhibited a more dramatic change in Li^+ rejection, decreasing from 33.5% to −53.2% (Fig. 5c, d). The negatively charged membranes yielded threefold higher $S_{Li^+/Mg^{2+}}$ than that of the positively charged membranes in high MLR solutions (Supplementary Fig. 23). This enhanced selectivity is primarily attributed to the fact that at high MLR, the increased concentration of Mg^{2+} on the surface of negatively charged membranes exacerbates the competition for water in the hydration shell of Li^+. In contrast, for positively charged membranes, Mg^{2+} predominantly remains in the concentration polarization layer, preventing any competitive effect that would induce Li^+ dehydration (Fig. 3e). Negative Li^+ rejection in positively charged membranes only emerges at high MLR, where co-ion competition driven by Donnan equilibrium becomes significant (Fig. 5d). The notable discrepancy in Li^+ rejection trends between positively and negatively charged membranes under high MLR conditions is challenging to rationalize using the theory of Cl^- preferential partitioning and its subsequent co-transport with Li^+ (Fig. 1e). The significant enhancement in separation performance, promoted by the counter-ion competition mechanism, showcases the unparalleled advantages of negatively charged membranes in practical lithium extraction applications.

Effects of membrane properties on counter-ion competition

We also investigated the impact of membrane characteristics on the separation performance of Li^+ and Mg^{2+} by fabricating negatively charged NF membranes with and without sulfonic groups (derived

from sodium sulfanilate, SS, Supplementary Fig. 24 and Supplementary Table 3). In addition, dodecyl phosphate (DDP) is primarily used in the organic phase to narrow the pore size and sharpen the pore size distribution (Supplementary Fig. 25)[23]. The differences in Li^+ rejection in mixed salt solutions for the membranes are illustrated in Fig. 5e and Supplementary Fig. 26. The presence of sulfonic groups results in a lower rejection towards Li^+ (from −1.6% to −18.3%), although there is also a minor reduction in Mg^{2+} rejection. To understand this behavior, we analyzed the interaction energies of the PIP-TMC unit (without sulfonic groups) and PIP/SS-TMC unit (with sulfonic groups) with Mg^{2+} and Li^+. Compared to the PIP-TMC unit, the interaction energies of Mg^{2+} and Li^+ with the PIP/SS-TMC unit were notably more negative, at −379.4 kcal mol^{-1} and −170.8 kcal mol^{-1}, respectively. This indicates a stronger affinity of the counter-ions with the sulfonic group-containing NF membranes (despite the PIP/SS-TMC membranes having slightly fewer negative charges, Fig. 5e). Additionally, divalent counter-ions like Mg^{2+} interact more strongly with the functional groups due to their higher charge compared to monovalent counter-ions like Li^+. However, for Mg^{2+} mass transfer, the highly uniform NF membrane allows for high Mg^{2+} rejection (>90%) through size exclusion. The increased enrichment of Mg^{2+} on the membrane surface further promotes the dehydration of Li^+. Moreover, the affinity of Li^+ to sulfonic group modulates the diffusion and transport behavior of Li^+ in solution and within the membrane, resulting in the membrane's low rejection capability for Li^+. Molecular snapshots and concentration profiles shown in Fig. 5g also indicate a higher concentration distribution of Li^+ on and within the PIP/SS-TMC/DDP NF membrane. This result further confirms that stronger binding energies favor the transport of monovalent counter-ions within the membrane, endowing the membrane with excellent separation performance.

Proof-of-concept lithium extraction

To demonstrate the effectiveness of the negatively charged NF membrane in treating real lithium brine, a chloride-type brine (composition detailed in Supplementary Table 4) from Xinjiang was employed, with its main ionic composition presented in Supplementary Fig. 27. The separation performance of the negatively charged NF membrane was evaluated using this complex brine matrix (see experimental details in Supplementary Section 1.5 and Supplementary Fig. 28 of the Supporting Information). The high concentration of impurity ions, particularly Na^+ (Supplementary Table 4), resulted in a Li^+ rejection of approximately 20% (Supplementary Fig. 29). The presence of high Na^+ concentration diminishes the Mg^{2+}-induced dehydration of Li^+ due to the lower hydration energy of Na^+ compared to Li^+, which makes Na^+ more prone to dehydration than Li^+ (Supplementary Table 5). Therefore, when a low concentration of Na^+ (equivalent to the concentration of Li^+, Supplementary Table 6) was introduced into the solution alongside Mg^{2+}, the DK membrane showed a −116.4% rejection for Na^+ (Supplementary Fig. 30). When the Na^+ concentration is lowered to a level comparable to that of Li^+, the competitive dehydration of Mg^{2+} against Li^+ is re-established, resulting in a reduction in Li^+ rejection (Supplementary Fig. 30). This phenomenon likely underpins the widespread use of NF as a post-processing step in selective adsorption technologies during lithium extraction from salt lakes. Importantly, the negatively charged membrane exhibited excellent antifouling ability against $CaSO_4$ compared to the positively charged membrane (Supplementary Fig. 31). By minimizing Li^+ rejection, negatively charged dense NF membranes not only maximize lithium recovery but also help maintain lithium purity during processing.

Discussion

In this study, we uncover an ion competition mechanism in NF membranes, driven by the counter-ion competition effect, which fundamentally reshapes our understanding of ion transmembrane selectivity. Using both commercially available and self-prepared NF membranes with varying charge characteristics, we demonstrate that charged membranes improve counter-ions separation during mixed-salt filtration. Specifically, the negatively charged membrane exhibits a 110% decrease in Li^+ rejection upon the introduction of Mg^{2+}, while SO_4^{2-} causes the positively charged PEINF membrane to shift Cl^- rejection from positive to negative. This phenomenon, where highly hydrated counter-ions reduce the rejection of weakly hydrated counter-ions in charged membranes, is termed the counter-ion competition effect. The counter-ion competition effect significantly enhances Li^+/Mg^{2+} separation in negatively charged dense NF membranes, a behavior not easily explained by the traditional Donnan effect. Molecular dynamics simulations confirm the dehydration phenomenon during mixed-salt filtration, revealing that a thinner hydration layer reduces the size exclusion effect on Li^+ and potentially strengthens its electrostatic attraction to the negatively charged NF membrane, thereby increasing Li^+ permeability. Additionally, ion diffusion coefficient measurements suggest that the counter-ion competition effect can be further amplified by the synergistic interplay of membrane charge and pore size.

Thanks to the counter-ion competition effect, the negatively charged dense NF membrane demonstrates a three-fold increase in $S_{Li^+/Mg^{2+}}$ in high MLR feed solutions compared to positively charged membranes. The combination of low Li^+ rejection and high $S_{Li^+/Mg^{2+}}$ enhance lithium recovery while maintaining lithium purity—an outcome more easily achieved with negatively charged dense NF membranes with controlled and uniform pore size. It is undeniable that under extremely acidic conditions (e.g., in spent lithium-ion battery recycling), the diminished (or even vanished) counter-ion competition effect may compromise the separation efficiency of conventional negatively charged polyamide NF membranes. Overall, this work uncovers an ion competition mechanism in NF membranes, offering practical insights for the development of advanced NF materials tailored for highly selective ion separation, particularly in lithium extraction from high-MLR salt-lake brines.

Methods

Membrane performance tests

A cross-flow filtration system (effective membrane area of 7 cm^2, feed tank volume of 1000 mL, purchased from Hangzhou Saifei membrane Co. Ltd., Zhejiang, China) was employed to evaluate the NF separation performance. Before testing, all membranes were pre-compacted at 6 bar to ensure steady-state stability. Subsequently, 2 mL of permeate was collected for further characterization. The solute rejections (%) were tested under a constant pressure of 5 bar at 25 °C, and the cross-flow velocity was 40 L h^{-1}. Rejection (%) was calculated as follows:

$$Rejection\ (\%) = \left(1 - \frac{C_p}{C_f}\right) \times 100 \tag{1}$$

where C_p and C_f refer to the solute concentrations in the permeate and feed, respectively.

The separation factor of Li^+ and Mg^{2+} was calculated by Eq. (2).

$$S_{Li^+/Mg^{2+}} = \frac{\frac{J_{Li}}{C_{f,Li}}}{\frac{J_{Mg}}{C_{f,Mg}}} = \frac{\frac{J_w \times C_{p,Li}}{C_{f,Li}}}{\frac{J_w \times C_{p,Mg}}{C_{f,Mg}}} = \frac{\frac{C_{p,Li}}{C_{f,Li}}}{\frac{C_{p,Mg}}{C_{f,Mg}}} = \frac{1 - \left(1 - \frac{C_{p,Li}}{C_{f,Li}}\right)}{1 - \left(1 - \frac{C_{p,Mg}}{C_{f,Mg}}\right)} = \frac{(1 - R_{Li^+})}{(1 - R_{Mg^{2+}})} \tag{2}$$

where J_{Li} and J_{Mg} are the permeation rates of Li^+ and Mg^{2+}, respectively. J_w is the water flux. R_{Li^+} and $R_{Mg^{2+}}$ are defined as the rejection of Li^+ and Mg^{2+}, respectively. $C_{p,Li}$ and $C_{p,Mg}$ stand for the concentrations (mg L^{-1}) of Li^+ and Mg^{2+} in the permeate, respectively.

Computational simulations

All molecular dynamics simulations were performed by Materials Studio 2017/R2 modeling (Accelrys Inc.) with the COMPASS III force field. The electrostatic interactions were calculated using the Ewald summation method and the van der Waals interaction. The cross-linked polyamide membrane to be simulated was prepared via a heuristic approach, where the cross-linking of monomers occurred based on distance criteria[39]. Initially, the amine monomers and acyl chloride monomers were randomly placed within a computational box with periodic boundary conditions, followed by geometric optimization with a maximum of 5000 iterations. Subsequently, the cross-linking reaction was initiated by controlling the distance between the carbon atom of the acyl chloride and the nitrogen atom of the amine. The simulation was conducted at a temperature of 300 K and a pressure of 1 bar under Andersen thermodynamics within the NVT ensemble. It was assumed that an amide bond would form, and HCl would be generated when the distance between the nitrogen and carbon atoms was less than 2.5 Å. Additionally, the cutoff radius was incrementally increased by 1 Å until the cross-linking reaction ceased, ultimately stopping when the cutoff radius reached 12.5 Å[40]. After the cross-linking process, the unreacted amines as well as the resulting HCl were removed, and the unreacted acyl chloride groups were converted into carboxylic acid groups. The membrane underwent further geometric optimization for 5000 steps and was equilibrated for 1 ns in the NPT ensemble (at 300 K and 1 bar), followed immediately by the NVT ensemble (1 ns, 300 K, 1 bar). Following these steps, the pore size distribution of the equilibrated membrane was analyzed using the script. The equilibrated membrane was then used in subsequent diffusion simulations to calculate interaction energies and diffusion coefficients. In detail, a box containing a 30 Å vacuum layer was modeled, with the feed solution placed above the cross-linked membrane. The feed solution was prepared by introducing Mg^{2+} and/or Li^+, Cl^- and H_2O. After structural optimization and equilibrium of the box, the membrane was fixed. Molecular dynamics simulations were performed in the NVT ensemble at 300 K, and the final snapshot was used for data analysis. Analysis involved the interaction energy between ions and the membrane, the density distribution of Mg^{2+} on the membrane surface, the RDF of Li^+ around the OW, and the diffusion coefficient of ions.

The interaction energy calculation, reflecting the interaction strength among the selected system components, is given by[25,41]:

$$E_{\text{int}} = E_{total} - \Sigma E_{componet} \tag{3}$$

where E_{total} and $E_{componet}$ denote the total electronic energy of the system and the electronic energy of each individual component in the system, respectively. The negative E_{int} value implies a stronger interaction attraction between the selected molecules.

The diffusion coefficient of ions can be derived from MSD and calculated using an Einstein equation[11,42]:

$$MSD = \frac{1}{N}\sum_{i=1}^{N}\left[r_i(t) - r_i(t_0)\right]^2 = A + 6D_a t \tag{4}$$

where $r(t)$ and $r(t_0)$ represent the position of a particle at time t and the initial time, respectively. D_a is the diffusion coefficient, calculated by converting the slopes of the MSD versus time curve.

Characterizations

Zeta potential of the membrane surface was analyzed by the potentiometric analyzer (SurPASS, Anton Paar Co., Austria). The chemical compositions and structure of the active layer were examined by X-ray photoelectron spectroscopy (XPS, ESCALAB 250Xi, Thermo Fisher Scientific Co., USA). The structure of the fouled NF membrane was characterized by energy dispersive spectrometer analysis under 20 kV accelerated voltage by field emission scanning electron microscopy (S-4800, Hitachi, Japan). An inductively coupled plasma optical emission spectrometry (ICP-OES, iCAP PRO, Thermo Fisher Scientific Co., USA) spectrometer and ion chromatography with the anion exchange column (Metrosep A Supp5 – 250/4.0, Metrohm, Switzerland) were used for determining of cations and anions concentrations in feeds and permeates, respectively. The concentrations of neutral molecules were determined by the high-performance liquid chromatography coupled with a refractive index detector (HPLC-RID, Agilent 1100 series, USA).

Reporting summary

Further information on research design is available in the Nature Portfolio Reporting Summary linked to this article.

Data availability

All data that support the findings of this study are available within the paper and its Supplementary Information or from the corresponding author upon request. Molecular dynamics trajectories were provided in an additional source data file. Source data are provided with this paper.

Code availability

The scripts for simulations performed in this study are available from the corresponding author upon request.

References

1. Lu, D. et al. Separation mechanism, selectivity enhancement strategies and advanced materials for mono-/multivalent ion-selective nanofiltration membrane. *Adv. Membr.* **2**, 100032 (2022).
2. Zhang, F., Fan, J. -b & Wang, S. Interfacial polymerization: from chemistry to functional materials. *Angew. Chem. Int. Ed.* **59**, 21840–21856 (2020).
3. Zhai, X., Lin, S., Li, X. & Wang, Z. The hidden role of the dielectric effect in nanofiltration: a novel perspective to unravel new ion separation mechanisms. *Environ. Sci. Technol.* **58**, 15874–15884 (2024).
4. Haddad, A. Z. et al. How to make lithium extraction cleaner, faster and cheaper - in six steps. *Nature* **616**, 245–248 (2023).
5. Peng, H. et al. Quaternization-spiro design of chlorine-resistant and high-permeance lithium separation membranes. *Nat. Commun.* **14**, 5483 (2023).
6. Fan, F. et al. A bioinspired membrane with ultrahigh Li^+/Na^+ and Li^+/K^+ separations enables direct lithium extraction from brine. *Adv. Sci.* **11**, 2402898 (2024).
7. Zhang, G. et al. Spontaneous lithium extraction and enrichment from brine with net energy output driven by counter-ion gradients. *Nat. Water* **2**, 1091–1101 (2024).
8. Zhang, Y. et al. Advances and promotion strategies of membrane-based methods for extracting lithium from brine. *Desalination* **566**, 116891 (2023).
9. Xu, P. et al. Positive charged PEI-TMC composite nanofiltration membrane for separation of Li^+ and Mg^{2+} from brine with high Mg^{2+}/Li^+ ratio. *Desalination* **449**, 57–68 (2019).
10. Hong, S. et al. Precision ion separation via self-assembled channels. *Nat. Commun.* **15**, 3160 (2024).
11. Xu, T. et al. Perfect confinement of crown ethers in MOF membrane for complete dehydration and fast transport of monovalent ions. *Sci. Adv.* **10**, eadn0944 (2024).
12. Guo, B.-B. et al. Double charge flips of polyamide membrane by ionic liquid-decoupled bulk and interfacial diffusion for on-demand nanofiltration. *Nat. Commun.* **15**, 2282 (2024).
13. Soyekwo, F., Wen, H., Liao, D. & Liu, C. Nanofiltration membranes modified with a clustered multiquaternary ammonium-based ionic

liquid for improved magnesium/lithium separation. *ACS Appl. Mater. Interfaces* **14**, 32420–32432 (2022).
14. Li, Z., Zhao, F., Chen, H., Yang, L. & Zhang, J. 3D electrospray printing PEI-TMC nanofiltration membrane for efficient and long-term stable separation of Mg^{2+}/Li+. *J. Membr. Sci.* **713**, 123373 (2025).
15. Li, J., Peng, H., Liu, K. & Zhao, Q. Polyester nanofiltration membranes for efficient cations separation. *Adv. Mater.* **36**, 2309406 (2023).
16. Peng, H. & Zhao, Q. A nano-heterogeneous membrane for efficient separation of lithium from high magnesium/lithium ratio brine. *Adv. Funct. Mater.* **31**, 2009430 (2021).
17. Lu, D. et al. Constructing a selective blocked-nanolayer on nanofiltration membrane via surface-charge inversion for promoting Li^+ permselectivity over Mg^{2+}. *J. Membr. Sci.* **635**, 119504 (2021).
18. Wu, H. et al. A novel nanofiltration membrane with [MimAP][Tf_2N] ionic liquid for utilization of lithium from brines with high Mg^{2+}/Li^+ ratio. *J. Membr. Sci.* **603**, 117997 (2020).
19. Xu, Y. et al. High performance Mg^{2+}/Li^+ separation membranes modified by a bis-quaternary ammonium salt. *Desalination* **526**, 115519 (2022).
20. Peng, H., Su, Y., Liu, X., Li, J. & Zhao, Q. Designing Gemini-electrolytes for scalable Mg^{2+}/Li^+ separation membranes and modules. *Adv. Funct. Mater.* **33**, 2305815 (2023).
21. Luo, J. & Wan, Y. Effects of pH and salt on nanofiltration - a critical review. *J. Membr. Sci.* **438**, 18–28 (2013).
22. Szoke, S., Patzay, G. & Weiser, L. Characteristics of thin-film nanofiltration membranes at various pH-values. *Desalination* **151**, 123–129 (2003).
23. Peng, Q. et al. Extreme Li-Mg selectivity via precise ion size differentiation of polyamide membrane. *Nat. Commun.* **15**, 2505 (2024).
24. Wang, L. et al. Significance of co-ion partitioning in salt transport through polyamide reverse osmosis membranes. *Environ. Sci. Technol.* **57**, 3930–3939 (2023).
25. Xu, R., Kang, Y., Zhang, W., Pan, B. & Zhang, X. Two-dimensional MXene membranes with biomimetic sub-nanochannels for enhanced cation sieving. *Nat. Commun.* **14**, 4907 (2023).
26. Doyle, D. A. et al. The structure of the potassium channel: molecular basis of K^+ conduction and selectivity. *Science* **280**, 69–77 (1998).
27. Gouaux, E. & MacKinnon, R. Principles of selective ion transport in channels and pumps. *Science* **310**, 1461–1465 (2005).
28. Zhang, L., Zhang, C., Dong, X. & Dong, Z. Highly selective transmembrane transport of exogenous lithium ions through rationally designed supramolecular channels. *Angew. Chem. Int. Ed.* **62**, e202214194 (2023).
29. Xu, P. et al. Charge-sign-independent separation of mono- and divalent ions with nanofiltration membranes. *Adv. Funct. Mater.* **35**, 2416458 (2024).
30. Dai, R. et al. Nanovehicle-assisted monomer shuttling enables highly permeable and selective nanofiltration membranes for water purification. *Nat. Water* **1**, 281–290 (2023).
31. Guo, H., Gao, X., Yu, K., Wang, X. & Liu, S. Ion adsorption on nanofiltration membrane surface and its effect on rejection of charged solutes: a zeta potential approach. *Sep. Purif. Technol.* **326**, 124830 (2023).
32. Madaeni, S. S. & Salehi, E. Adsorption of cations on nanofiltration membrane: separation mechanism, isotherm confirmation and thermodynamic analysis. *Chem. Eng. J.* **150**, 114–121 (2009).
33. Garcia-Aleman, J. & Dickson, J. M. Permeation of mixed-salt solutions with commercial and pore-filled nanofiltration membranes: membrane charge inversion phenomena. *J. Membr. Sci.* **239**, 163–172 (2004).
34. Zhai, X., Wang, Y.-L., Dai, R., Li, X. & Wang, Z. Roles of anion–cation coupling transport and dehydration-induced ion–membrane interaction in precise separation of ions by nanofiltration membranes. *Environ. Sci. Technol.* **56**, 14069–14079 (2022).
35. Lu, C. et al. Dehydration-enhanced ion-pore interactions dominate anion transport and selectivity in nanochannels. *Sci. Adv.* **9**, eadf8412 (2023).
36. Chen, Z. et al. Steric hindrance-induced dehydration promotes cation selectivity in trans-subnanochannel transport. *ACS Nano* **17**, 12629–12640 (2023).
37. Shefer, I., Peer-Haim, O., Leifman, O. & Epsztein, R. Enthalpic and entropic selectivity of water and small ions in polyamide membranes. *Environ. Sci. Technol.* **55**, 14863–14875 (2021).
38. Roth, R. S. et al. Effect of solution ions on the charge and performance of nanofiltration membranes. *npj Clean. Water* **7**, 25 (2024).
39. Li, N., Li, M., Lin, S., Cui, S. & Zhang, X. Stoichiometric effect on the structural transformation and spatial variation of polyamide reverse osmosis membranes: a molecular dynamics study. *J. Membr. Sci.* **686**, 121980 (2023).
40. Wang, Q., Hu, L., Ma, H., Venkateswaran, S. & Hsiao, B. S. High-flux nanofibrous composite reverse osmosis membrane containing interfacial water channels for desalination. *ACS Appl. Mater. Interfaces* **15**, 26199–26214 (2023).
41. Gao, S.-L. et al. Comparative analysis of polyamide nanofiltration membranes resistance to different acids: insights from experiments and density functional theory simulations. *J. Membr. Sci.* **694**, 122412 (2024).
42. Shen, L. et al. Polyamide-based membranes with structural homogeneity for ultrafast molecular sieving. *Nat. Commun.* **13**, 500 (2022).

Acknowledgements

This research was financially supported by the National Natural Science Foundation of China (22278406, J.L.) and the National Key Research and Development Program of China (2021YFC3201402, Y.W.).

Author contributions

L.L. designed the experiments, carried out experiments, performed molecular dynamics simulation and wrote the original draft. S.L. revised the manuscript and developed the theory. X.X. performed molecular dynamics simulation and revised the manuscript. Y.W. and W.S. supervised the project and supported Funding. J.L. conceived the idea, revised the manuscript, supervised the project and supported Funding.

Competing interests

The authors declare no competing interests.

Additional information

Supplementary information The online version contains supplementary material available at https://doi.org/10.1038/s41467-025-61336-6.

Correspondence and requests for materials should be addressed to Yinhua Wan or Jianquan Luo.

Peer review information *Nature Communications* thanks Zhe Yang and the other anonymous reviewer(s) for their contribution to the peer review of this work. A peer review file is available.